PROPORTIONAL-COUNTER SELECTION OF CLOUD-CHAMBER EVENTS

Thesis by

Carl Albert Rouse

In Partial Fulfillment of the Requirements

for the Degree of

Doctor of Philosophy

California Institute of Technology

Pasadena, California

1956

ACKNOWLEDGEMENTS

The author wishes to acknowledge those who have made this thesis possible. With deep and sincere pleasure, the author wishes to express his thanks to Professor Carl D. Anderson and Professor Eugene W. Cowan for their continuing interest, inspiration and guidance. Their many fruitful suggestions concerning every phase of this work are largely responsible for the success of the experiment.

The author is also very grateful to Drs. Robert B. Leighton, Victor A. J. van Lint, George H. Trilling, Arnold A. Strassenburg, John D. Sorrels, Don Pickerell, Messrs. John Kadyk, Robert Luttermoser, Gerry Neugebauer, Fred Fuselier, Edward Williams, Bruce Dean and Robert Blocker for the part each had in the design, construction and operation of the 48" magnet-cloud chamber; construction of the proportional counter; and helping the author understand the associated electronic circuits. The cooperation and productivity of everyone associated with the Cosmic Ray Laboratory left the author with a deep sense of pride in having been a part of the group.

In addition to Drs. Anderson and Cowan, the author wishes to thank Drs. Leighton, Trilling, and Robert F. Christy for several stimulating discussions concerning various parts of the data obtained during the experiment.

Finally, for direct and indirect financial aid, the

author is indebted to the California Institute of Technology for the awarding of the Paul E. Lloyd Fellowship; the physics department for part-time employment and a Graduate Assistantship; Mrs. Margaret Fleming who very kindly allowed the author to occupy her patio house (and use her swimming pool) during the greater part of his stay at the institute; and to the Office of Naval Research for their financial support of the research.

ABSTRACT

The 48" magnet-cloud chamber has been controlled by a gated proportional counter and photographs taken of 5313 expansions have been analyzed.

The proportional counter was found to (1) select events of lower energy than penetrating shower detectors; and (2) select at a much lower hourly rate interactions in which V-particles were produced. However, the V-particles detected appeared on the average to be of lower energy, hence, could be measured with maximum cloud-chamber accuracy.

The μ-meson-induced electron showers detected by the proportional counter have been analyzed. Experimental and theoretical frequencies were obtained for the production of showers with a minimum of 40, 100, and 200 electrons. The frequencies for showers of 100 and 200 electrons were found to be the most reliable. These experimental frequencies are $1.6^{+0.8}_{-0.4} \times 10^{-6}$ per second and $0.44 \pm 0.21 \times 10^{-6}$ per second, respectively. The corresponding theoretical values computed from collision and bremsstrahlung probabilities for spin $\frac{1}{2}$ μ-mesons of 10×10^{-6} per second and 3.5×10^{-6} per second reflect the uncertainties of cascade shower theory.

Two V-particles of particular interest were photographed. One, event 47202, appears to be strong evidence for the existence of the neutral τ-particle with the decay scheme, $\tau^{o} \rightarrow \pi^{+} + \pi^{-} + \pi^{o} + Q \sim 78$ Mev.

The second V-particle, event 46944, was a negatively charged K-particle that is consistent--from ionization-momentum measurements and decay dynamics--with the decay scheme, $\Theta^- \rightarrow \pi^- + \pi^0$, P* = 206 Mev/c. The measured P* for the event is 207 $\pm$ 10 Mev/c. With other events that could be consistent with the Θ^-, this event helps to establish the existence of this K-particle.

TABLE OF CONTENTS

		Page
I.	INTRODUCTION	1
II.	PROPORTIONAL-COUNTER SELECTION WITH THE 48" MAGNET-CLOUD CHAMBER	4
	A. APPARATUS	4
	B. RESULTS	6
	C. SUMMARY AND CONCLUSIONS	12
III.	PENETRATING SHOWER DETECTION	15
	A. INTRODUCTION	15
	B. RESULTS	15
IV.	COMPARISON OF PROPORTIONAL COUNTER AND PENETRATING SHOWER SELECTION	17
V.	μ-MESON INDUCED ELECTRON SHOWERS	20
	A. INTRODUCTION	20
	B. EXPERIMENTAL RESULTS	20
	C. THEORETICAL DISCUSSION	25
	D. DISCUSSION OF RESULTS	31
	E. SUMMARY AND CONCLUSIONS CONCERNING μ-MESON ELECTRON SHOWERS	33
VI.	NEUTRAL K-PARTICLE	34
	A. INTRODUCTION	34
	B. MEASUREMENTS AND ANALYSIS	34
	C. CONCLUSIONS	43
VII.	CHARGED K-PARTICLE	44
	A. INTRODUCTION	44
	B. MEASUREMENTS AND ANALYSIS	44
	C. SUMMARY AND CONCLUSIONS	48
VIII.	APPENDIX	49
	APPENDIX A	49
	APPENDIX B	51
IX.	REFERENCES	59

I. INTRODUCTION

There are two basic ways in which expansion-type cloud chambers may be operated: (a) random selection of events (1,2,3) or (b) controlled selection of events (1,4,5). With random expansions it is difficult to make the sensitive time of the chamber greater than 1/1000th to 1/200th of the total time of operation even with short recycling times, large volumes, and long sensitive times. The advantage of a randomly operated cloud chamber is its lack of bias on the observed events. The two main disadvantages are (a) the low efficiency for the selection of interesting events and (b) the low accuracy of measurements when the event does not immediately precede the time when the chamber is photographed. Thus, the present need for large numbers of interesting events with accurate measurements makes some form of cloud chamber control necessary.

Control of the chamber has been done by various forms of particle detectors in various arrangements about the cloud chamber. The detectors have been arranged externally, internally or in a combination external-internal array. The particular geometry used necessarily introduces a bias toward particular types of events in the set of photographs obtained. There is also a bias due to the rigor of selection used, i.e., the types and amounts of absorber used and the numbers of detectors required in coincidence and/or

anti-coincidence in order to record the event. Hence, in designing a cloud-chamber experiment, the 'counter' geometry and 'counter' coincidence--anti-coincidence is chosen to give the most efficient collection of the events under investigation.

The particle detectors used for cloud-chamber control have taken several forms. Geiger counters (6,7,8), scintillation counters (9), fast ion chambers (10,11), Čerenkov detectors (12,13,14), π-μ decay detectors (15), neutron counters (16,17,18), and proportional counters (19,20,21) have been used in various manners and with varying degrees of success. Of these the Geiger-counter selection has been by far the most productive. Nevertheless, the particles of interest observed in the high-energy interactions selected by penetrating shower detectors usually have high momenta in the laboratory system of reference. Hence, identification of the particles through accurate ionization-momentum measurements and observation of decay modes is difficult with the magnetic fields and chamber sizes available. The bias of penetrating-shower detectors thus passes low-momenta and perhaps other types of events that are, or could be, of interest. With this in mind, other investigators have tried the above mentioned Čerenkov detectors, scintillation counters, neutron counters, π-μ decay detectors, skeleton proportional counters (19), and standard thin-walled, gas-filled proportional counters in an attempt to photograph

low-energy events or other events of interest. After operating a thin-walled proportional counter in a six-inch magnet-cloud chamber (20), it was decided to build one for the 48" magnet-cloud chamber. The events obtained with the 48" chamber are analyzed below and compared with a sample of events detected with the same apparatus triggered with penetrating shower detection. Of particular interest is the analysis of μ-meson-induced electron showers and a neutral K-particle and a charged K-particle that decay in the chamber.

II. PROPORTIONAL-COUNTER SELECTION WITH THE 48" MAGNET-CLOUD CHAMBER

A. APPARATUS

The 48" magnet-cloud chamber has been described in the theses of Drs. Victor A. J. van Lint (22) and George H. Trilling (23). The electronic circuits for the proportional counter were basically those used by Drs. M. L. Merritt (20) and R. C. Jopson (21). Consequently it is only necessary to briefly describe the proportional counter and the chamber geometry used during the present experiment.

The proportional counter was of the thin-walled gas-filled type, being constructed of .010-in. brass and filled to 44 psi (absolute pressure) Argon and 0.5 psi CO_2. Supporting ribs maintained the rectangular shape of the counter. The counter was 1 in. thick, 3 in. wide, and 10 in. long with a 1-mil tungsten wire placed along the 10-in. axis acting as the anode.

A schematic drawing of the chamber geometry is shown in Fig. 1. Note particularly the location of the proportional counter between the middle and bottom cloud chambers.

The expansion of the chamber was controlled by a coincidence of any one of six Geiger counters in the shielded counter tray between the top chamber and the middle chamber and a proportional-counter pulse of a size corresponding to a particle of about four times minimum ionization. This

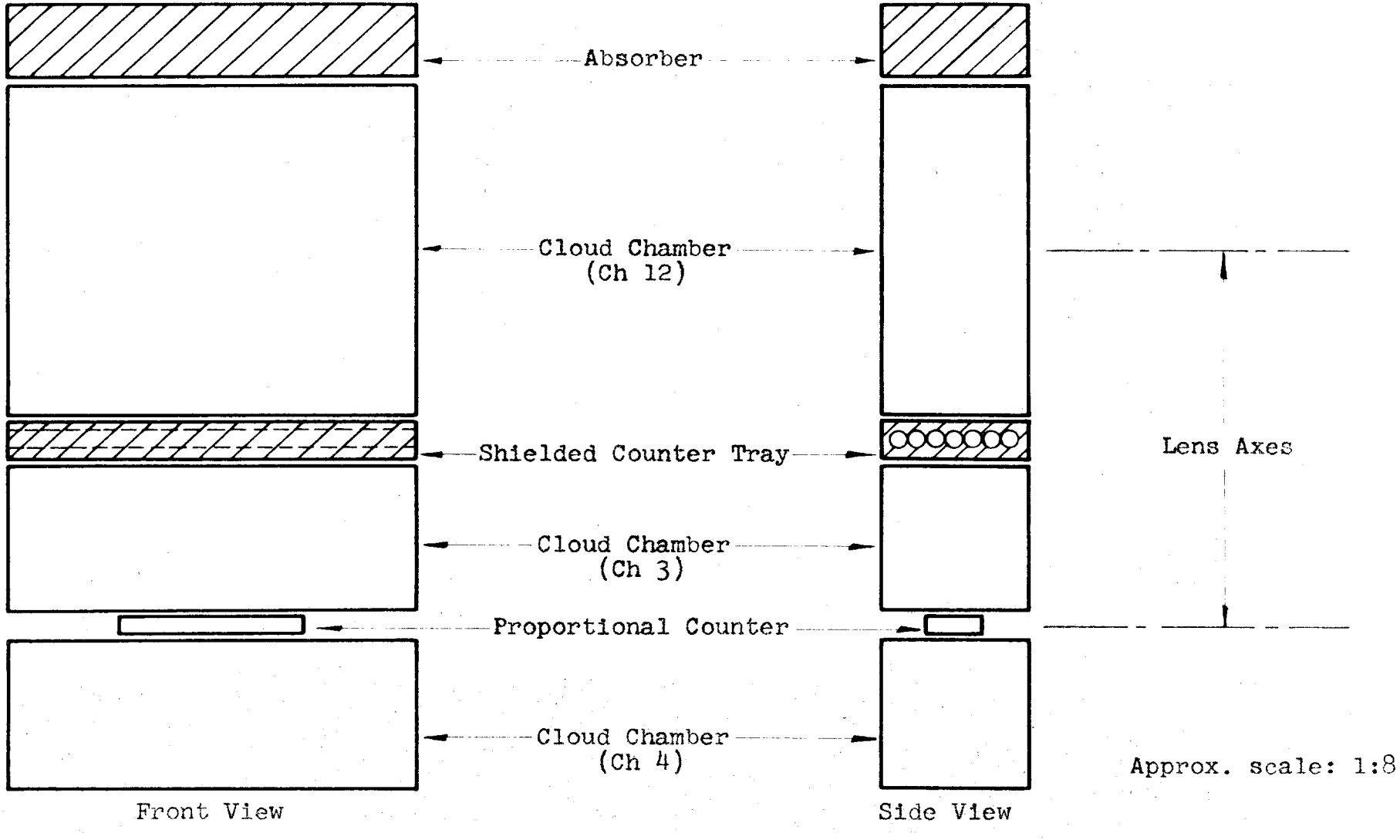

Fig. 1. Schematic diagram of the cloud-chamber geometry.

ionization is that of about four 1 Mev/c electrons, a 67 Mev/c π-meson, or a 230 Mev/c K-particle. (The cloud chambers will henceforth be referred to, from top to bottom, as Ch 12, Ch 3, and Ch 4.) Because of the difficulty of accurately determining the minimum pulse height necessary to trip the chamber, the circuit adjustments were chosen as a function of the picture-taking rate. A rate of about three pictures per hour was found to be optimum for this investigation. After each expansion, a three-minute hold time permitted the chambers to return to equilibrium.

The photography, thermostating, and measurement techniques were the same as described by van Lint (22).

B. RESULTS

Tables I through IV summarize the events selected during the last 1476 hours of operation. A total of 4203 pictures were taken at an over-all average rate of 2.9 per hour. Faster and slower rates were used for two rolls of film. However, this produced no significant changes in the hourly rates for the various events. Tables II, III, and IV expand on items listed in Table I.

In Table I, 'Stars', 'Penetrating Showers', 'Electron Showers' and 'Mixed Showers' are self-explanatory. 'Stopping or Stars' are events in which a track is visible in Ch 3 above the proportional counter but not visible in Ch 4 below the counter. Observation in Ch 4 would have been possible if there were no intervening absorber. If the momentum of

these tracks were $\geq$200 Mev/c, the event was listed as a 'Probable Star' in Table III. The 'μ-meson-induced electron showers' are events in which a single track was observed in Ch 12 and associated with it an electron shower produced in the lead and observed in Ch 3. Fig. 3 is the photograph of a large electron shower produced by a μ-meson. (Cf. Section V.)

Table IV separates the 'Miscellaneous' events. From an examination of this Table the difficulties of proportional-counter operation are evident. The high percentage of single tracks tripping the chamber was probably due to a combination of reasons. Fluctuation in the ionization of the track (20) while passing through the proportional counter; knock-on electrons occurring within the proportional counter; and amplifier noise or 110 volt line transients occurring during the gate time and added to a "minimum-ionizing" pulse from the proportional counter appear to be the most probable causes.

Included in the 'Accidental' pictures were all pictures in which no visible particle was observed passing through the proportional counter. In many of these pictures, electrons were seen coming from the back pistons of Ch 3 or Ch 4, hence not all of the accidentals were due to noise or pulse-height variations. Corrections in the amplifier circuit reduced the number of accidentals from as high as 65 per cent in one preliminary roll to an average of 10 per cent in later

Table I. Summaries of events obtained with proportional-counter and penetrating-shower detection.

Event	Proportional-counter selection* No.	%	/hr	Penetrating-shower selection** No.	%	/hr
Decaying V-particles	11***	0.28	0.009	20	3.0	0.13
Stars	231	5.5	0.185	23	3.4	0.15
Stopping or Stars	160	3.8	0.13	12	1.8	0.078
Penetrating showers	26	0.62	0.021	90	13.3	0.59
Electron showers	440	10.5	0.35	26	3.8	0.17
μ-meson-induced electron showers	92	2.2	0.074	5	0.74	0.033
Mixed showers	105	2.5	0.084	13	1.9	0.085
Pictures with at least one track with $I \geq 1.7\ I_o$	272	6.5	0.22	75	11.0	0.49
Miscellaneous	2965	70.0	2.4	548	81.0	3.6

* Sensitive time: 1250 hrs.

** Sensitive time: 153 hrs.

*** Does not include events 46944 and 47202.

Table II. Decaying V-particles.

Type V-particle	Proportional-counter selection			Penetrating-shower selection		
	No.	%	/hr	No.	%	/hr
Λ^{o}	4	36	0.0032	4	20	0.026
θ^{o}	1	9	0.0008	4	20	0.026
V^{+}	-	-	-	1	5	0.0065
V^{-}	2	18	0.0016	2	10	0.013
V^{o}	4	36	0.0032	9	45	0.059
Totals	11	100	0.009	20	100	0.13

Table III. Stars detected during proportional-counter selection.

Origin	No.	%	/hr
Proportional counter	124	41.0	0.10
Absorber between Ch 12 and Ch 3	77	25.5	0.062
Absorber between Ch 3 and Ch 4 (outside proportional counter)	18	6.0	0.014
Absorber above Ch 12	12	4.0	0.01
Probable stars (tracks stopping in proportional counter)	71	23.5	0.057
Totals	302	100.0	0.265

Table IV. Miscellaneous events detected during proportional-counter selection.

Event	No.	% of misc.	% of total	/hr
Singles	1861	62.8	42.0	1.5
Doubles	202	6.8	4.8	0.16
Triples	22	0.8	0.5	0.018
Knock-on electrons from proportional counter	147	5.0	3.5	0.12
Accidentals	625	21.0	14.8	0.50
Blank	75	2.5	1.8	0.06
Chamber did not expand	33	1.1	0.8	0.026
Totals	2965	100.0	70.0	2.37

rolls. Such a reduction was necessary for the success of the experiment.

Table II lists the decaying V-particles observed in the cloud chambers during the experiment. Four of the V-particles were produced in stars originating in the proportional counter, as shown in the photograph, Fig. 2. This represents about one V-particle per 50 to 60 such stars if the 71 'Probable Stars' of Table III are included, or, one V-particle per 30 to 40 proportional-counter stars if the 'Probable Stars' are not included. In addition, approximately 10 or more tracks from the stars appeared to be consistent with non-decaying charged K-particles. Several of them could possibly have been stopped had there been plates in Ch 4. Of the V-particles observed during the entire experiment the most interesting are events 47202 and 46944, which are discussed in Sections VI and VII, respectively. The first appears to be strong evidence for the existence of the τ^{o}, and the second is an excellent case of a Θ^{-}.

C. SUMMARY AND CONCLUSIONS

The following observations and conclusions were drawn from the present experiment:

1. Events 46944, 47202, 51035, and others; μ-meson-induced electron showers; and several low-angle penetrating showers show that gated proportional-counter control of an expansion cloud chamber selects interesting events that are

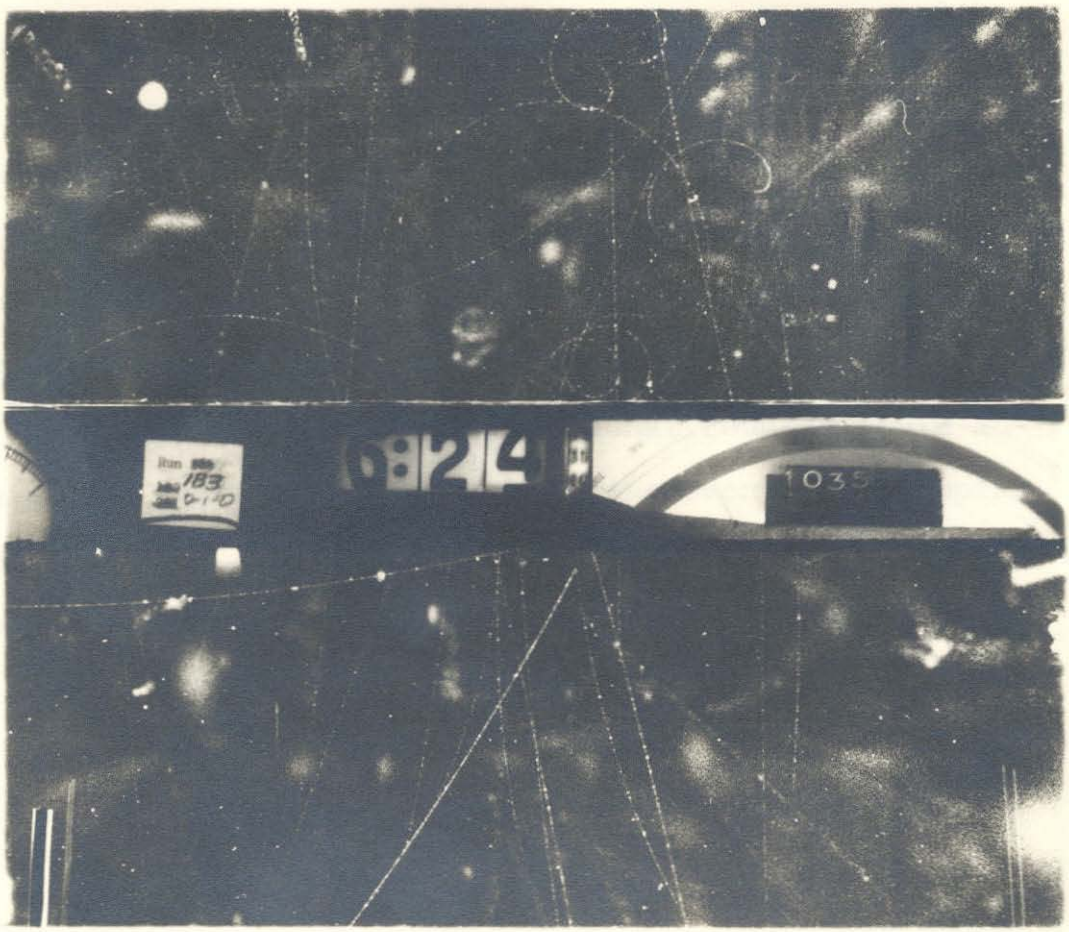

Fig. 2. Event 51035. Λ° emitted from a 'proportional counter' star. This penetrating shower is outside the solid angle of the penetrating-shower detector.

passed or detected with less certainty by penetrating shower detectors.

2. In the 124 'proportional-counter' stars, only about four contained more than five high-energy tracks within a small angle. This seems to indicate that proportional counters do select low-energy interactions. A complete analysis, however, has not been made.

3. Plates below the proportional counter would increase the observation of interesting events by stopping the long-lived, low-energy, unstable particles produced in the 'proportional-counter' stars.

III. PENETRATING-SHOWER DETECTION

A. INTRODUCTION

Cloud-chamber geometry for penetrating-shower detection is that shown in references (22) and (23). It is the same as that shown in Fig. 1 except for the following three changes:

(a) Shielded Geiger-counter tray used above Ch 12.

(b) A lead absorber 1-5/8 in. thick placed between Ch 3 and Ch 4 in place of the proportional counter.

(c) Shielded Geiger-counter tray placed below Ch 4.

The characteristics of penetrating-shower detectors are well known. Hence, this section is not meant to be an exhaustive study of a large number of pictures. Only 677 pictures from three recent rolls of film were surveyed in order to get some numbers for a qualitative comparison with the proportional-counter results discussed above.

B. RESULTS

The 677 pictures were taken during a sensitive time of 153 hours with an average picture-taking rate of 4.4 per hour. The chamber was triggered by either of two types of coincidences: 0-2-2 or 2-2-1. This means that any simultaneous pulses occurring from 0 (or 2) counters in the top counter tray, 2 (or 2) or more counters in the middle tray,

and 2 (or 1) or more counters in the bottom tray will cause the event to be photographed. The results are listed in Tables I and II along with the proportional-counter results. Only the V-particles are discussed in detail since the events of interest in Tables III and IV do not apply to penetrating-shower detection. In Table I, the events listed carry the same meaning as described above in Section II, Part B, except for 'Miscellaneous.' The 548 pictures classed as 'Miscellaneous' in penetrating-shower detection are all pictures in which there is no evidence of a shower--penetrating, mixed, or electron. The events, however, cannot be classified as accurately as the proportional-counter events in Table IV with respect to the efficiency of the detecting technique. It is interesting to notice that two of the 20 V-particles and about 30 to 50 per cent of the stars and stopping particles were observed in pictures in which there was no visible evidence of a shower.

IV. COMPARISON OF PROPORTIONAL-COUNTER AND PENETRATING-SHOWER SELECTION

From the hourly rates listed in Table I, one can draw the following conclusions:

1. Penetrating-shower detection is much more efficient as a detector of decaying V-particles. Nevertheless, events like 46944, 47202, and 51035 indicate that proportional-counter selection has a better chance per V-particle of detecting cases that can be measured with maximum accuracy.

2. Stars are observed with about the same frequency. However, in Table III note that almost half of the stars detected during proportional-counter selection were produced in the much smaller amount of absorber immediately above, within, or immediately below the proportional counter. Using the value of 6.7 grams per square centimeter, a star frequency of about 0.016 stars per cubic centimeter per day is obtained. The 110 grams per square centimeter in the two lead absorbers within the cloud chamber used during penetrating-shower selection result in a frequency of observation of about 0.00048 stars per cubic centimeter per day. (Stopping tracks were not included in the calculations.)

3. Penetrating showers are detected with greater efficiency with penetrating-shower detectors, although the gated-proportional counter has a better chance of detecting low-angle penetrating showers. In addition to event 47202,

there were two other events in which such low-angle shower secondaries produced interactions in the bottom of Ch 12, from which tracks consistent in mass with K-particles traversed the height of the chamber. Such events produced in plates below a proportional counter would probably have been accompanied by a decay above the counter.

4. Electron showers are detected with greater efficiency with proportional counters.

5. Mixed showers are detected with about equal efficiency.

6. μ-meson-induced electron showers are detected with greater efficiency with proportional-counter selection.

7. More of the events photographed with penetrating-shower selection have at least one track with ionization greater than about 1.7 times minimum ionization visible in the chamber volume.

8. About ten per cent more events of those photographed with penetrating shower selection were triggered by events other than showers, stars or stopping particles, such as single particles.

From the experiment, it was concluded that:

1. Gated proportional counters require more attention than Geiger counters, but, it was found that after the amplifier-noise and line-transient problems were reduced, the apparatus operated with a relatively high degree of stability. In fact, during the last half of the experiment, the major source of the maintenance problems was not the proportional

counter and its circuits, but the rest of the cloud-chamber apparatus.

2. Gated proportional counters used in magnet-cloud chamber geometry similar to that of this experiment, can best be used under the following conditions:

(a) With good 110-volt line filtering.

(b) With large proportional-counter area and with two or more anodes within the sensitive volume of the proportional counter.

(c) In parallel with penetrating-shower detectors.

V. μ-MESON INDUCED ELECTRON SHOWERS

A. INTRODUCTION

The most extensive investigation of electromagnetic interactions of μ-mesons has been the experiments by M. Schein and P. S. Gill (24) on "bursts" detected in shielded ionization chambers. R. F. Christy and S. Kusaka (25) did the theoretical analysis of the results. Other experiments are given in references (31) and (32). Similar events were observed in the 48" magnet-cloud chamber with proportional-counter control. Fig. 3 shows an example of a μ-meson-induced electron shower containing 200 or more electrons. Cloud-chamber data of such events have the advantage over previous ionization-chamber measurements in that effects of stars and air showers are not included.

B. EXPERIMENTAL RESULTS

Table V lists the relative sizes and frequencies of the 92 showers reported in Table I. In Table V, 'S' is the minimum number of electrons observed in the shower and 'N(S)' is the number of showers with S or more electrons. The common logarithm (written in this section as 'log') of these values is plotted in Fig. 4 in a graph of log N(S) vs log S. The slope of this graph beyond S=40 is consistent with that obtained by Schein and Gill (24). The decreased

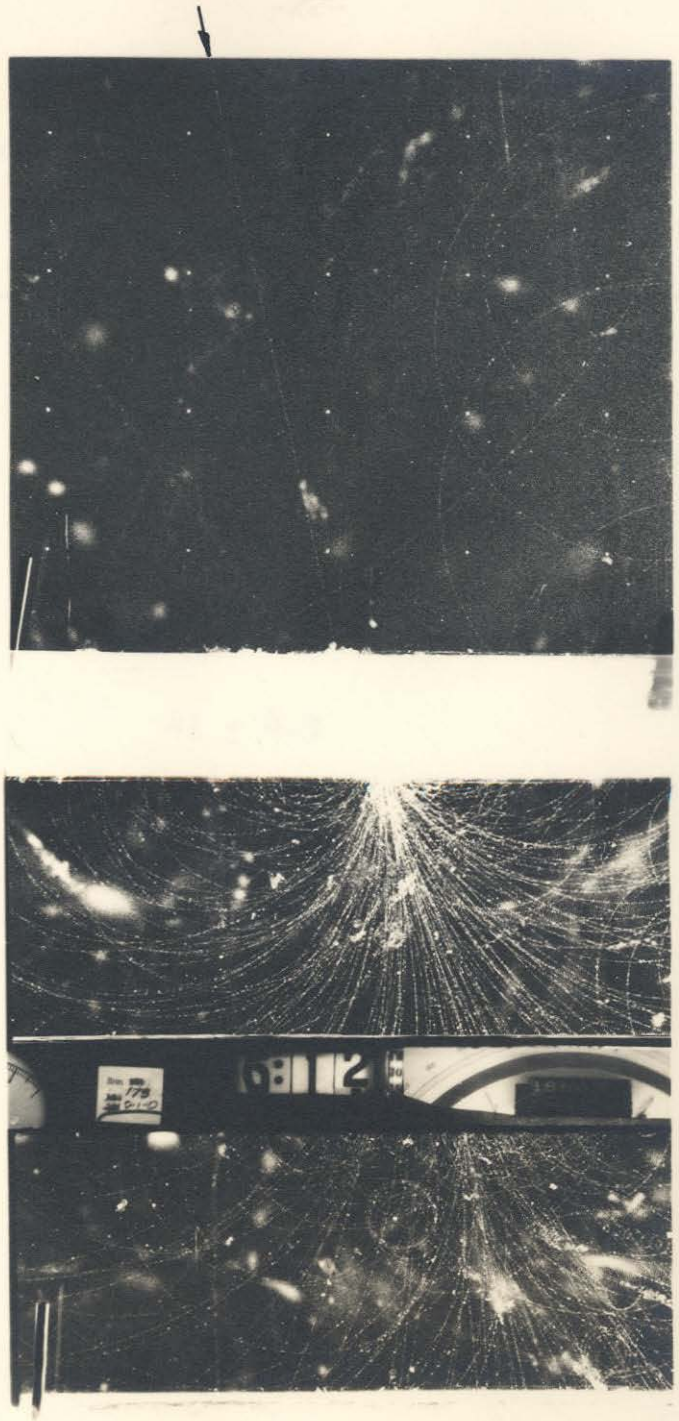

Fig. 3. Event 48668. μ-meson-induced electron shower. About 200 or more electrons are visible in the middle cloud chamber.

Table V. Frequencies of μ-meson-induced electron showers.

S*	N(S)**	Frequency (/hr)
10	92 ± 6.5	0.074
15	65 ± 5.4	0.052
20	56 ± 5.0	0.045
25	46 ± 4.5	0.037
30	41 ± 4.3	0.033
40	31 ± 3.7	0.025
50	21 ± 3.1	0.017
60	15 ± 2.6	0.012
70	10 ± 2.1	0.0080
100	7 ± 1.8	0.0056
200	2 ± 0.95	0.0016

* Minimum number of electrons observed in the shower.

** Number of showers with S or more electrons.

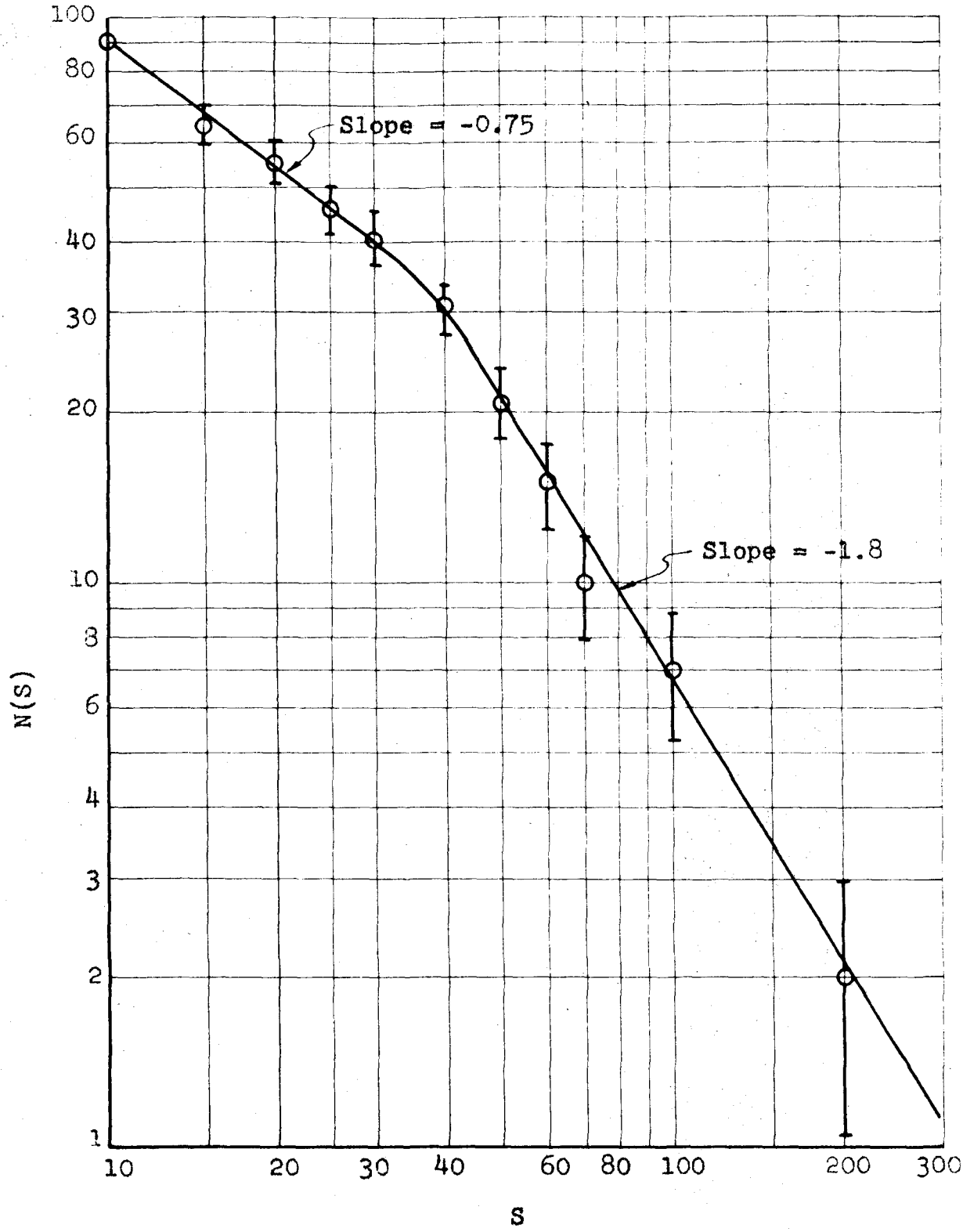

Fig. 4. Graph of log N(S) vs. log S.

slope below S = 40 probably reflects a decreasing efficiency of detection more than anything else.

The frequencies at which the showers for particular values of S were observed during the sensitive time of 4.5 x 10^{-6} seconds are as follows:

S	N(S)	N(S)/sec ($\times 10^{-6}$)
40	31 $\pm$ 3.7	6.8 $\pm$ 0.8
100	7 $\pm$ 1.8	1.6 $\pm$ 0.4
200	2 $\pm$ 0.95	0.44 $\pm$ 0.21

The primaries of all the showers passed through an area of 690 square centimeters at a distance of 39 centimeters above the proportional counter. The horizontal area of the proportional counter is 190 square centimeters. These quantities do not exactly define the exact total solid angle but from the pictures it was decided that they give a fair approximation.

After considering the theory of such showers these experimental results will be discussed in more detail.

C. THEORETICAL DISCUSSION

The theoretical frequency for the production of electron showers of S electrons by electromagnetic interaction of μ-mesons in ten radiation lengths of lead is given by (cf. Christy (25)):

$$N(S)/_{sec} = X_o \int_{E_{omin}}^{\infty} \int_{E'_{min}}^{E'_{max}} \int_{t=0}^{t=10} N(E_o) \Phi_{\substack{col \\ rad}}(E_o,E') P(E',t,S)\, dt\, dE'\, dE_o \qquad (1)$$

where separate integrations are carried out for the contributions of collision and radiation processes to the frequency and where

E_o -- μ-meson energy in Bev.

E' -- Energy of knock-on electron or energy of radiated photon in Bev.

t -- Depth of absorber in radiation lengths.

X_o -- Radiation length in gram per cm^2.

$N(E_o)dE_o \approx \frac{15.8}{E_o^3} dE_o$ -- Number of μ-mesons per second with energy E_o in dE_o admitted in the solid angle of the experimental geometry (28).

$\Phi_{col}(E_o,E')dE'$ -- Probability per gram per cm^2 that a μ-meson of energy E_o will produce a knock-on electron of energy E' in dE'.

$\Phi_{rad}(E_o,E')dE'$ -- Probability per gram per cm^2 that a μ-meson of energy E_o will radiate a photon of energy E' in dE'.

$P(E',t,S)$ -- Probability that a knock-on electron or photon of energy E' at depth t will produce a shower of S or more electrons at depth $t = 10$.

E'_{max} -- $E_o^2/(E_o + 11)$ is the maximum transferable energy by a μ-meson of energy E_o.

E'_{min} -- Minimum energy of a knock-on electron or photon that will produce a shower of S electrons at depth t = 10.

E_{omin} -- Energy of a μ-meson whose maximum transferable energy is the minimum energy of a knock-on electron or photon that will produce a shower of S electrons at a depth t = 10, or, a μ-meson whose $E'_{max} = E'_{min}$.

Christy and Kusaka computed Φ_{col} and Φ_{rad} for a particle of mass m, of spin 0, $\frac{1}{2}$, and 1 and of "normal" magnetic moment. The forms of the above probabilities for particles of spin $\frac{1}{2}$ and mass m given by Rossi (26) and used here with the same notation are

$$\Phi_{col}(E_o,E')dE' = \frac{2Cm_e c^2}{\beta^2} \frac{dE'}{(E')^2} \left[1 - \beta^2 \frac{E'}{E'_{max}} + \tfrac{1}{2}\left(\frac{E'}{E_o + mc^2}\right)^2\right],$$

and

$$\Phi_{rad}(E_o,E')dE' = \frac{4\alpha NZ^2}{A} r_e^2 \left(\frac{m_e}{m}\right)^2 \frac{dE'}{E'} \left[1 + (1 - \frac{E'}{E_o})^2 - \frac{2}{3}(1 - \frac{E'}{E_o})\right]$$

$$\left[\ln\left(\frac{2E_o^2 h}{m^2c^3 r_n} \frac{\left(1 - \frac{E'}{E_o}\right)}{E'}\right) - \tfrac{1}{2}\right],$$

where $C = \pi NZr_e^2/A = 0.150Z/A$ cm^2/gm and $r_n = 1.38 \times 10^{-13} A^{\frac{1}{3}}$ cm $= 0.49\, r_e A^{\frac{1}{3}}$, r_e = electron radius. For the energies of interest, $\beta = 1$.

The probability P(E',t,S) was obtained by the use of Rossi shower curves (27) shown in Fig. 5. An example of the

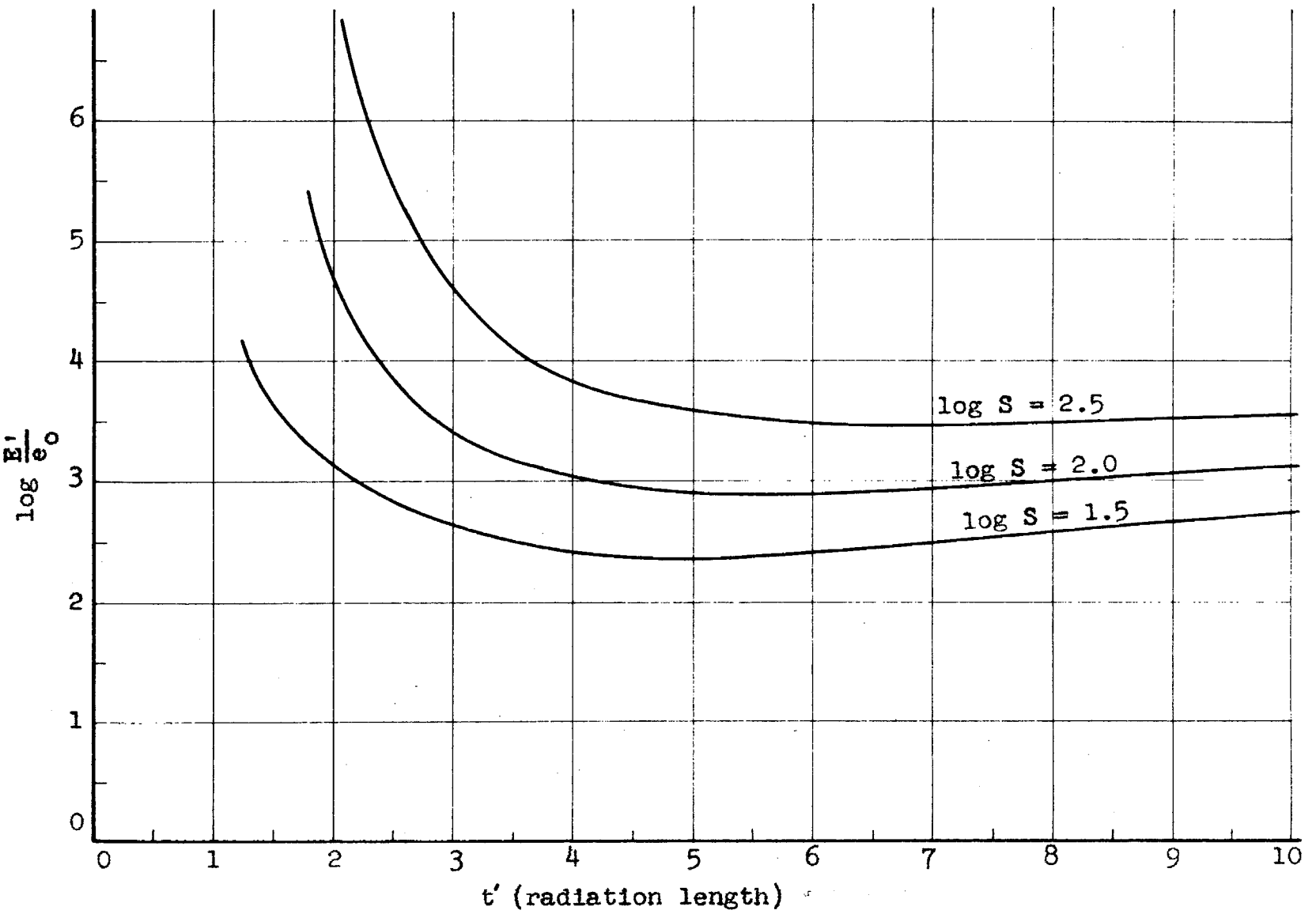

Fig. 5. $\log \frac{E'}{e_o}$ vs t', for different values of S (cf. reference (27)).

method will be given by finding the probability for the production of 100-electron showers by knock-on electrons or photons of 7.5 Bev energy. Fig. 6 shows the graph of $P(E',t,S)$ vs t obtained by the following approximate method. The ten radiation-length absorber is divided into five cells of two radiation lengths, each cell centered about t = 1,3,5, 7, and 9. Consider now Fig. 5. For showers of 100 electrons, the curve labeled log S = 2 is the curve of interest. Only small fluctuations in S--order of magnitude $S^{\frac{1}{2}}$--are assumed. Using the critical energy e_o = 0.0076 Bev, log (E'/e_o) is 2.99, for E' = 7.5 Bev. The critical energy, e_o, is the collision loss per radiation length of electrons of energy e_o. The next step is to note where the value of log (E'/e_o) lies with respect to the curve, log S = 2, at the various values of t' (t' = 10-t). For the knock-on occurring at t = 3, the value of log (E'/e_o) = 2.99 is noted in Fig. 5 at t' = 7, since t' = 7 is now equivalent to t = 10 in the absorber. The value lies essentially on the curve, hence the probability for this cell is 0.5 since half of the time S would be greater than 100 and half of the time, less. For t = 5 in the absorber; at t' = 5 in Fig. 5 the value of log (E'/e_o) lies above the curve, hence the probability is 1.0 for this cell. For the other cells, the value of log (E'/e_o) lies below the curve, hence the value of $P(E',t,S)$ is zero for these cells. Consequently, the outline of the shaded area in Fig. 6 represents the ap-

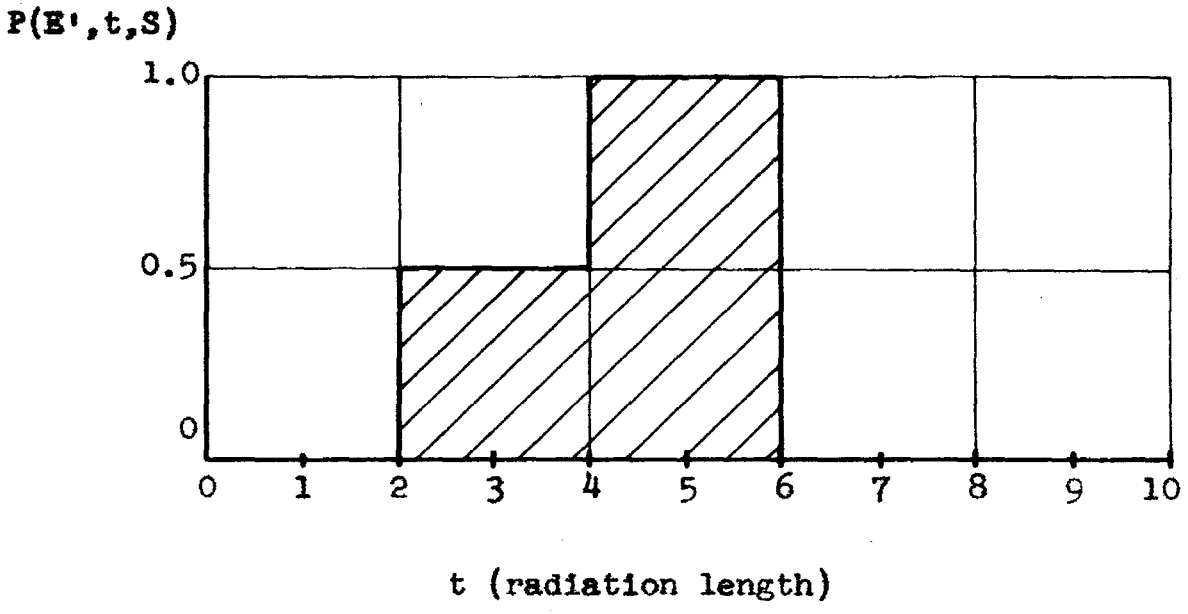

Fig. 6. Graph of P(E',t,S) vs t, for E' = 7.5 Bev and S = 100 electrons.

proximate function $P(E',t,S)$ for $E' = 7.5$ Bev and $S = 100$. The probability functions for other values of E' were obtained in a like manner.

Because of the nature of $P(E',t,S)$, Eq. (1) had to be integrated numerically. Eq. (1) then becomes

$$N(S)/\text{sec} \approx \chi_o \sum_{\Delta E_o\, \Delta E'\, \Delta t} \sum \sum N(E_o) \oint_{\substack{\text{col} \\ \text{rad}}} (E_o, E') \, P(E',t,S) \, \Delta t \, \Delta E' \, \Delta E_o$$

where the summation is carried out over Δt, $\Delta E'$, and ΔE_o between the limits of integration given in Eq. (1). An upper limit of 200 Bev was used in the summation over E_o since the contribution to the frequencies beyond this is negligible. Using reasonable values of E' and E_o, approximate theoretical frequencies were obtained as follows (with the experimental values repeated beside them for comparison):

S	Experimental frequency ($\times 10^{-6}$/sec)	Theoretical frequency ($\times 10^{-6}$/sec)	Ratio of theoretical to experimental frequency
100	1.6 ± 0.4	10	6
200	0.44 ± 0.21	3.5	8
40	6.9 ± 1.7	68	10

In an attempt to account for the large discrepancies between the experimental and theoretical frequencies, two factors were varied independently to test the effect on the theoretical values. First, the value of the critical energy, e_o, was raised to 10 Mev and the calculations carried through for showers of 100 or more electrons. This reduced the above theoretical frequency about 40 per cent to about 6×10^{-6} per second.

Next, with e_o still equal to 7.6 Mev, it was assumed that the observed showers of 100 or more electrons corresponded to calculated showers of 200 or more electrons. This would be the theoretical frequency for the 200-electron showers above, i.e., 3.5×10^{-6} per second. This is about a 65 per cent reduction in this theoretical frequency. Physically, this assumption is based on the loss of electrons in the absorber by scattering and perhaps other causes. The experiments of W. Blocker *et al.* (33) indicate that this loss due to back-scattering is about 41 per cent of the calculated number of electrons. Consequently, varying both factors at once could conceivably reduce the theoretical number to about $2\text{-}3 \times 10^{-6}$ per second.

Another uncertainty is the size and position of the shower maximum in lead. Belenky (34) shows that these quantities are smaller than those used in the Rossi shower curves. This change would decrease the theoretical frequencies further a few per cent.

Finally, the final uncertainty considered is the amount of the fluctuations in the size of the showers. The fluctuations are believed to range anywhere from $S^{\frac{1}{2}}$ to S-1 (29). Larger fluctuations than those assumed in this analysis would cause an increase in the theoretical frequency due mainly to the contributions by fluctuations below E'_{min} and E_{omin}. The actual value is probably somewhere between the values above.

D. DISCUSSION OF RESULTS

The major sources of error in the experimental results are as follows:

1. Knowledge of the μ-meson spectrum. The best values available to the author of the vertical intensities of μ-mesons of various energies were obtained by the use of two graphs listed by J. G. Wilson (28). One graph is a range--energy relation for μ-mesons in terms of range through earth, in meters of water. The second graph is that of the vertical intensity of the hard component of cosmic radiation as a function of depth through earth.

2. Poor statistics for S = 100 and S = 200.

3. Decreased efficiency of detection for the smaller electron showers. A momentum of about 50 to 60 Mev/c is needed for an electron leaving the lead absorber above Ch 3 in a vertical direction to reach the proportional counter. Without materialization of photons in the brass absorber above the proportional counter, the detection of the event would depend on the possible causes for single tracks tripping the chamber discussed in Section II, Part B, above.

4. Difficulty of observing every electron that enters Ch 3, particularly in large showers. This error will always be in one direction, viz., to give a value of S that is actually smaller than the minimum number of electrons in the class of showers. Therefore, the error in the experimental

shower frequency for S = 100 should perhaps be $1.6^{+0.8}_{-0.4} \times 10^{-6}$ per second rather than as given on page 24.

The major factors influencing the accuracy of the theoretically derived cross-sections are:

1. Knowledge of the μ-meson spectrum as above.

2. Complexity of the theoretical analysis of cascade electron showers (cf. Rossi (29)).

3. The uncertainties of cascade shower theory.

4. The effect of a magnetic field on the development of a cascade electron shower. The exact analysis of this would be quite complex, but the effect is believed to be small.

5. The accuracy of the probability function, P(E',t,S). Its accuracy depends on (2) through (4) above and the finite size of the cells used.

E. SUMMARY AND CONCLUSIONS CONCERNING μ-MESON ELECTRON SHOWERS.

The following conclusions can be made about μ-meson-induced electron showers:

1. Cloud chambers controlled by proportional counters afford a better method for the study of μ-meson electromagnetic interactions than ionization chambers.

2. The large discrepancy between the experimental and theoretical shower frequencies appear to reflect the uncertainties in shower theory, particularly the critical energy, loss of electrons due to scattering, size and position of the shower maximum, and fluctuations in the sizes of the showers.

VI. NEUTRAL K-PARTICLE

A. INTRODUCTION

The decay in Ch 12 of a neutral K-particle--event 47202--is shown in Fig. 7. The cloud chamber was triggered by the low-angle penetrating shower visible in the lower-left corner of the chamber. The axis of the shower is down to the right and toward the piston of the chamber. There appears to be an almost equal probability of triggering the chamber by either penetrating-shower detection or gated-proportional-counter control, but perhaps a greater probability should be given to the proportional counter because of the direction of the shower axis. The V-particle appears to have been produced in the interaction in the bottom of Ch 12, well defined by the three heavily ionizing tracks seen originating on the bottom left side of the chamber. This apparent origin is indicated by the arrow at 'O' in the figure.

B. MEASUREMENTS AND ANALYSIS

In Fig. 7, the positive track is indicated by the arrow at 'A' and the negative track, by the arrow at 'B'. The momentum of the positive was determined to be 101 $\pm$ 3 Mev/c and that of the negative track, 93.6 $\pm$ 3 Mev/c, with an included angle of 61.8°. The ionization estimates for each

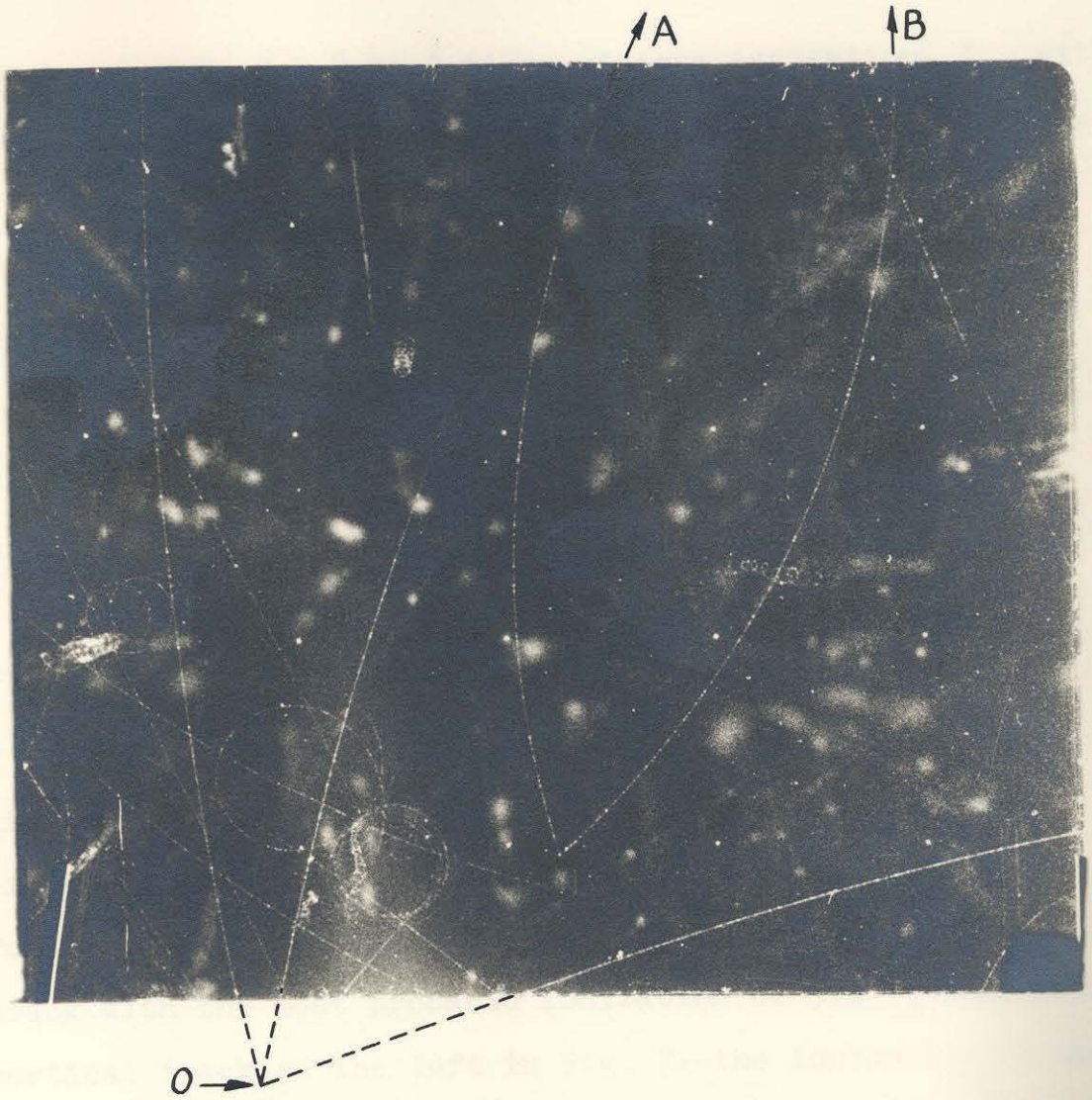

Fig. 7. Event 47202. Decay of a neutral K-particle that appears to be strong evidence for the existence of a neutral τ-particle with the decay scheme, $\tau^{o} \rightarrow \pi^{+} + \pi^{-} + \pi^{o} + Q \sim 78$ Mev.

track range from 1.8 to 3 times minimum ionization, I_o, with the most probable values of ionization, I, given by 2.5 I_o.

In order to get the most probable masses of the particles, a comparison of the expected values of ionization for π-mesons and μ-mesons of momenta P_+ = 101 Mev/c and P_- = 94 Mev/c are made as follows:

	P_+ 101 Mev/c	P_- 94 Mev/c
π-meson	2.3 I_o	2.5 I_o
μ-meson	1.7 I_o	1.8 I_o

Differences in ionization of 20 per cent or more should be discernible, but no difference that large is apparent. Further, by comparison with the identified, 520 Mev/c proton track with the most probable ionization of 3.0 I_o--the nearly vertical track on the left in Fig. 7--the ionization of the above tracks could not be lower than 2 I_o. Consequently, from ionization-momentum measurements, both particles are probably of π-meson mass. Their masses are certainly not as light as that of an electron.

Nevertheless, the dynamics of the decay were carried out considering three possible combinations of charged particles, viz., (π^+, π^-), (π^+, μ^-), and (μ^+, π^-). On the basis of a two-body decay, the three Q-values are obtained as follows:

$$Q(\pi^+,\pi^-) = 17.2 \pm 2.5 \text{ Mev} \quad (1)$$

$$Q(\pi^+,\mu^-) = 19.9 \pm 2.5 \text{ Mev} \quad (2)$$

$$Q(\mu^+,\pi^-) = 25.2 \pm 3.0 \text{ Mev} . \quad (3)$$

The resultant momentum, P_o, of the two visible tracks is 167 ± 4 Mev/c.

All three of the above Q-values are very different from that of the nomal θ^o decay,

$$\theta^o \rightarrow \pi^+ + \pi^- + Q \sim 214 \text{ Mev},$$

hence, the event is of the anomalous type reported by van Lint (22) and others. Three possible decay schemes that could explain the event are:

$$\tau^o \rightarrow \pi^+ + \pi^- + \pi^o + Q_{\tau^o} , \quad (4)$$

$$\theta^o_{anom} \rightarrow \pi^+ + \mu^- + \nu + Q_1 , \quad (5)$$

$$\theta^o_{anom} \rightarrow \mu^+ + \pi^- + \nu + Q_2 , \quad (6)$$

where ν is a neutrino. The highly probable origin can be used in an attempt to determine which decay scheme is the most probable. With an origin it is possible to simplify the analysis of a three-body decay to that of a two-body decay by considering the two visible tracks as a single particle of momentum equal to the vector sum of the momenta of the visible particles and of mass equal to the sum of the masses of the visible decay products plus the Q-value ob-

tained on the basis of a two-body decay. This method simplifies and completes the analysis of cascade three-body decays discussed by van Lint (22). (See Appendix A.)

Applying this method of analysis to event 47202, the masses of the 'combined' particles are, using relationships (1) through (6),

$$m_{\pi\pi} = 2m_{\pi} + 17 = 297 \text{ Mev} ,$$
$$m_{\pi\mu} = m_{\pi} + m_{\mu} + 20 = 266 \text{ Mev} ,$$
$$m_{\mu\pi} = m_{\mu} + m_{\pi} + 25 = 271 \text{ Mev} ,$$

with a laboratory momentum of

$$P_{\pi\pi} \equiv P_{\pi\mu} \equiv P_{\mu\pi} \equiv P_{o} = 167 \pm 4 \text{ Mev/c} .$$

If the vector representing the line of flight of the K^{o}-particle is called $\overrightarrow{LOF}$, then the angle between $\overrightarrow{P_{o}}$ and $\overrightarrow{LOF}$ is

$$(\overrightarrow{P_{o}}, \overrightarrow{LOF}) = 40.2^{o}$$

from which the transverse momentum is given by

$$P_{oT} = P_{o} \text{sine } 40.2^{o} = 108 \pm 3 \text{ Mev/c}$$

and the longitudinal momentum is given by

$$P_{oL} = P_{o} \text{cosine } 40.2^{o} = 127 \pm 3 \text{ Mev/c} .$$

Only the analysis of the τ^{o} decay will be discussed in detail. First, a minimum Q-value is obtained by assuming

that the transverse momentum is equal to the center-of-mass momentum, P^*_o, or

$$P_{oT} = P^*_o = 108 \text{ Mev/c} ,$$

Next, a π^o is assumed to be emitted with a momentum in the center-of-mass system equal and opposite to that of the $m_{\pi\pi}$, or,

$$\overrightarrow{P^*_{\pi^o}} = -\overrightarrow{P^*_o} .$$

Now the total energy of both particles in the center-of-mass system equals the minimum value for the rest mass of the parent particle and is given by

$$m_{min} = \sqrt{P^{*2}_{\pi^o} + m^2_{\pi^o}} + \sqrt{P^{*2}_o + m^2_{\pi\pi}} = 489 \text{ Mev} .$$

The minimum Q-value is then given by

$$Q_{min} = 489 - 2m_\pi - m_{\pi^o} = 74 \text{ Mev} .$$

In the decay of a τ^o of mass 493 Mev, the expected Q-value is 78 Mev. This implies that if the neutral particle in event 47202 is indeed of π^o mass, it is emitted at nearly right angles to the line of flight in the center-of-mass system--the most probable region of emission (22).

If, now an initial mass of 493 Mev is assumed, $P^*_{\pi^o}$ becomes 112 Mev/c. Using Trilling's formula (23) for $\gamma\beta$,

$$\gamma\beta = \frac{P_{oL} E^*_{\pi\pi} \pm E_{\pi\pi} P^*_{oL}}{m^2_{\pi\pi} + P^2_{oT}} \approx \frac{P_{oL} E^*_{\pi\pi}}{m^2_{\pi\pi} + P^2_{oT}} = 0.40$$

from which $\beta = 0.37$ and $\gamma = 1.08$ and

$$P_{\tau^o} = \gamma\beta m_{\tau^o} = 197 \text{ Mev/c} .$$

The time of flight is given by

$$t = \frac{|\overrightarrow{LOF}| \, m_{\tau^o}}{c \, P_{\tau^o}} = 1.9 \times 10^{-9} \text{ seconds} .$$

Finally, the minimum β for the event is

$$\beta_{min} = \frac{P_{oL}}{E_{\pi\pi}} = 0.37 .$$

Obviously, the event, relative to the visible origin, is very consistent with the assumption of the decay

$$\tau^o \rightarrow \pi^o + \pi^+ + \pi^- + Q \sim 78 \text{ Mev} .$$

Table VI lists the above quantities together with those for the decay schemes (5) and (6). Evidently, if we disregard ionization estimates, the dynamics can be consistent with all three decay schemes. The production dynamics, however, would favor the lowest value of β. The argument proceeds as follows. If no large fraction of the momentum of the primary production particle is absorbed by the nucleus, the velocity of a particle in the Laboratory System becomes increasingly smaller as the laboratory angle of emission becomes larger. Consider the relationship for the labora-

Table VI. Summaries of three possible three-body decay schemes for event 47202.

	(π^+,π^-,π^o)	(π^+,μ^-,ν)	(μ^+,π^-,ν)
Q-value (two-body decay) (Mev)	17 ± 2.5	19.9 ± 2.5	25.2 ± 3.0
'Combined' mass (Mev)	297	266	271
Minimum Q-value (Mev)	74	150	154
P* (Mev/c)	112	175	173
θ* (Degrees)	90	142	141
$\gamma\beta$(*)	0.40	1.02	0.98
β	0.37	0.72	0.70
γ	1.08	1.42	1.40
β_{min}	0.37	0.43	0.40
P(of K^o)(Mev/c)	197	504	485
Time of flight (x 10^{-9} seconds)	1.9	0.54	0.56

(*) All values of $\gamma\beta$ are single-valued.

tory momentum of a particle 'i' as a function of the laboratory angle of emission, θ_i, given by (30)

$$P_i(\theta_i) = \frac{P_i^*}{\gamma(1-\beta^2\cos^2\theta_i)}\left\{\frac{\beta}{\beta_i^*}\cos\theta_i \pm \sqrt{1-\frac{\left(\frac{\beta}{\beta_i^*}\right)^2-\beta^2}{1-\beta^2}\sin^2\theta_i}\right\},$$

where it is seen that for fixed β and β_i^*, P_i is a decreasing function of θ_i. In an interaction in which the velocity of the particle in the center-of-mass system (β_i^*) is equal to the velocity of the center of mass, the limiting laboratory angle of emission is 90° with a laboratory momentum equal to zero. The degree to which this is applicable to event 47202 depends on the fraction of the momentum absorbed by the nucleus in which the V-particle was produced. The magnitude of the probability that a large fraction of this momentum is absorbed by the nucleus can be ascertained from the total number of identified Λ°-particles produced in the absorbers between the cloud chambers during previous experiments. Of about 100 such particles observed, only about six were seen moving backward in the laboratory system.* Hence, the probability that the nucleus will absorb a large fraction

---

* It can be shown that in a nucleon-nucleon or π-nucleon collision, a product particle with mass greater than nucleon mass would not be seen traveling backward in the Laboratory System. See Appendix B.

of the momentum is less than .06. Now, the K^{o} under consideration appears to have been emitted at nearly right angles to the shower axis, hence, has the largest probability of having the lowest of the three possible values of β.

C. CONCLUSIONS

The following conclusions can be drawn concerning event 47202:

1. The masses of either particle observed in the decay of the particle shown in Fig. 7 is certainly not as light as the mass of an electron.

2. The analysis of event 47202 presents the strongest evidence known to the author for the existence of a neutral τ-particle with the decay scheme

$$\tau^{o} \rightarrow \pi^{+} + \pi^{-} + \pi^{o} + Q \sim 78 \text{ Mev} .$$

3. Because of the lack of observable evidence of the π^{o}, other possible decay schemes cannot be ruled out absolutely. A few more events of the quality of event 47202 (or better) are needed to firmly establish the existence of the τ^{o}.

VII. CHARGED K-PARTICLE

A. INTRODUCTION

One of the three negatively charged V-particles detected during the proportional-counter operation of the 48" magnet-cloud chamber is shown in Fig. 8. The particle entered the visible region of Ch 12 from the left-rear as indicated by the arrow at 'A' in the figure. It traversed about two-thirds of the chamber width and decayed near the rear-to-front center of the chamber. The visible secondary left the chamber as indicated by the arrow in the figure at 'B'. The chamber was triggered by low-energy particles that apparently came from the same interaction in which the particle of interest was produced. It appears that the event would have certainly been passed by the penetrating-shower detector.

B. MEASUREMENTS AND ANALYSIS

The momentum of the primary was determined to be 521 ± 40 Mev/c, and that of the seconday, 191 ± 7 Mev/c. The ionization of the primary is estimated to be about 1.5 times minimum ionization. The ionization of the secondary is estimated to be less than that of the primary and about 1.3 or 1.4 times minimum ionization. Now, the ionization

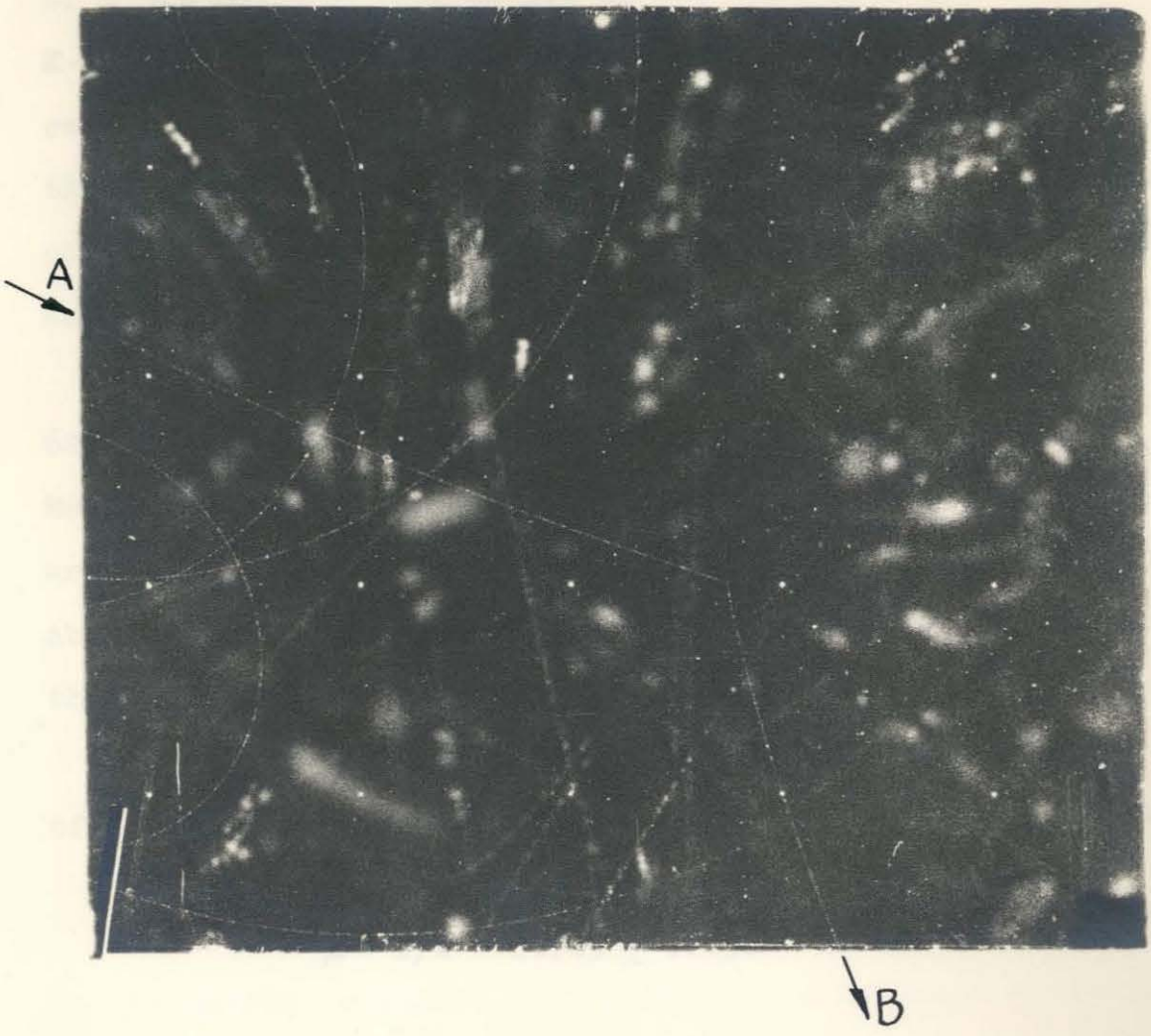

Fig. 8. Event 46944. Decay of a negatively charged V-particle that is consistent with the decay,

$$\theta^- \rightarrow \pi^- + \pi^o \text{ , } P^* = 206 \text{ Mev/c.}$$

P* for the event = 207 $\pm$ 10 Mev/c.

of a 520 Mev/c proton is 3.0 I_o and that of a 520 Mev/c K-particle is 1.5 I_o. Hence, the mass of the primary is certainly not greater than the mass of a proton. Further, the ionization of a 191 Mev/c π-meson is 1.25 I_o, and that of a 191 Mev/c μ-meson is 1.1 I_o. Consequently, the visible secondary is probably of π-meson mass.

The laboratory angle of emission of the π-meson is 62.2^o. From this, a transverse momentum, P_T, of 169 $\pm$ 6 Mev/c and a longitudinal momentum, $P_{L(\pi)}$, of 89 $\pm$ 3 Mev/c are obtained. The apparent length of the primary track is about 27 centimeters, hence, the time of flight is greater than 9×10^{-10} seconds.

Using the primary momentum of 521 Mev/c and a mass of 493 Mev, the velocity of the Center of Mass is given by

$$\beta = P/W = 0.725 \pm 0.056$$

where W is the total energy of the particle. From β,

$$\gamma\beta = 1.05 \pm 0.08$$

and

$$\gamma = 1.45 \pm 0.11 \ .$$

Transformation of $P_{L(\pi)}$ to the center of mass system gives

$$P^*_{L(\pi)} = \gamma P_L - \gamma\beta E_\pi = -120 \text{ Mev/c} ,$$

and with P_T determined above,

$$P^* = \sqrt{(P^*_L)^2 + (P_T)^2} = 207 \text{ Mev/c} .$$

Computation of the error in P* by the relationships given in reference (23) gives a ΔP^* of ± 10 Mev/c, or,

$$P^* = 207 \pm 10 \text{ Mev/c} .$$

The expected P* in the decay

$$\Theta^- \rightarrow \pi^- + \pi^0 + Q \sim 218 \text{ Mev}$$

is 206 Mev/c. Further, if the secondary of event 46944 is assumed to be a μ meson, a P* of 198 $\pm$ 10 Mev/c is obtained. This value is inconsistent with the expected value of P* of about 239 Mev/c for the decay

$$K^-_\mu \rightarrow \mu^- + ? + ? .$$

C. SUMMARY AND CONCLUSIONS

The following conclusions can be made concerning event 46944:

1. The mass of the primary is certainly not greater than the mass of a proton and most probably equal to the mass of a K-particle.

2. The event is inconsistent with the decay

$$K_{\mu}^{-} \rightarrow \mu^{-} + ? + ? \ ,$$

because of the difference of the measured and expected P* of about four probable errors.

3. The event shows excellent consistency with the decay

$$\theta^{-} \rightarrow \pi^{-} + \pi^{o} + Q \sim 218 \text{ Mev} \ .$$

4. With the cases reported by Trilling (23) in his study of charged V-particles and the others obtained in this laboratory since his report was written, the excellent case reported here helps to establish the existence of the θ^{-}.

VIII. APPENDIX

APPENDIX A

FURTHER COMMENTS ON CASCADE THREE-BODY DECAYS

Consider the decay of a particle of mass m_i that decays into two particles with masses m_o and m_1. Further, assume the particle m_o immediately decays into two more particles with masses m_2 and m_3. The cascade can be represented by the relationships as follows using the definition of a Q-value:

$$Q_{io} = m_i - m_1 - m_o \hookrightarrow m_2 + m_3 \ .$$

The second decay can also be written as

$$m_o = m_2 + m_3 + Q_{23} \ ,$$

or, substituting in and rearranging the above relationships,

$$m_i = m_1 + m_o + Q_{io}$$

$$= m_1 + m_2 + m_3 + Q_{23} + Q_{io}$$

and

$$m_i - m_1 - m_2 - m_3 = Q_{23} + Q_{io} = Q$$

Let m_2 and m_3 represent two measurable charged particles. Then Q_{23} is obtained from measurements on particles 2 and 3. With an assumed mass for m_1 and an origin, a minimum Q-value can be obtained after a minimum value for the mass of the primary particle, m_i, is determined from the relationship

$$m_{i(min)} = \sqrt{P_T^2 + m_o^2} + \sqrt{P_T^2 + m_1^2} \quad .$$

With this,

$$Q_{min} = m_{i(min)} - m_1 - m_2 - m_3 \ .$$

APPENDIX B

LIMITING LABORATORY ANGLE OF EMISSION OF HYPERONS

After it was noticed that only a small fraction of the observed neutral V-particles where seen moving backward in the laboratory system, the question of the production dynamics necessary for this was thought to be of interest.

Fig. 9 represents the collision of a particle of mass m_i and momentum P_i with a particle at rest of mass m_o. The particle of interest will be the product particle of mass m and laboratory momentum, P_m. The second particle of 'mass' M represents the sum of the masses of all the particles except the particle of interest plus the "Q-value" for these particles (e.g., mass m_o in Appendix A). P_M is their resultant momenta. The laboratory angle of emission of particle m is represented by θ_m--the other quantity of interest. The problem can now be restated as follows: For $m > m_o$, under what conditions will $\theta_m > 90^o$?

Consider, now, the transformation of the longitudinal component of the center-of-mass momentum of particle m given by

$$P_{mL} = \gamma P^*_{mL} + \gamma\beta W^*_m , \qquad (1)$$

where, of course, W_m is the total energy of the particle.

LABORATORY SYSTEM

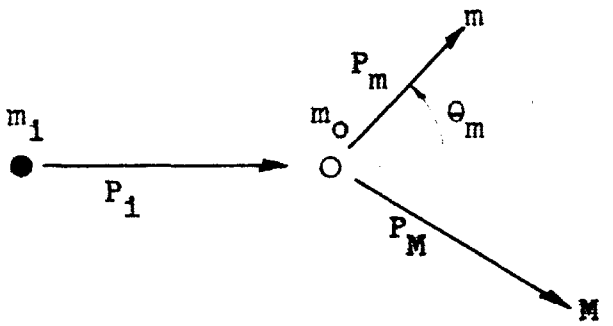

CENTER OF MASS SYSTEM

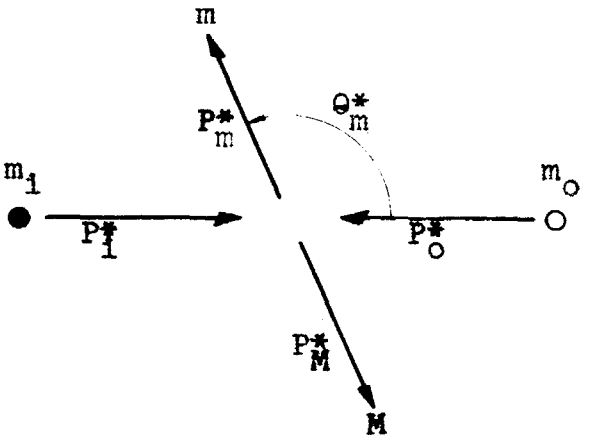

Total momentum = $\vec{P} = \vec{P}_i$

Total energy = $W = \sqrt{P_i^2 + m_i^2} + m_o$

Velocity of center of mass = $\vec{\beta} = \frac{\vec{P}_i}{W}$

$\vec{P}^*_m = -\vec{P}^*_M$

$W^* = \sqrt{P^{*2}_m + m^2} + \sqrt{P^{*2}_M + M^2}$

$P^{*2}_m = \left(\frac{W^{*2} + (M^2 - m^2)}{2W^*}\right)^2 - M^2$

$W = \gamma W^*$

Fig. 9. Schematic diagrams of a two-particle collision.

Calling the direction of P_i the positive direction, P_{mL} will be negative--which will be the case when m is emitted backward in the laboratory system--when P^*_{mL} is negative, and when $|\gamma P^*_{mL}| > \gamma\beta W^*_m$. The minimum value of P^*_m for which this could be true occurs when $P^*_{mL} = P^*_m$. Consequently, the problem reduced to that of finding the condition under which

$$\gamma P^*_m > \gamma\beta W^*_m$$

or

$$P^*_m > \beta W^*_m \tag{2}$$

The problem can be made more general by the analysis of the conditions under which

$$\beta W^*_m \gtreqless P^*_m \begin{cases} >, & \theta_m < 90^\circ \\ =, & \theta_m = 90^\circ \\ <, & \theta_m > 90^\circ \end{cases} \tag{3}$$

Squaring Eq. (3),

$$\beta^2 W^{*2}_m \gtreqless P^{*2}_m$$

or

$$\beta^2(P^{*2}_m + m^2) \gtreqless P^{*2}_m ,$$

transposing

$$m^2 \gtreqless \frac{(1-\beta^2)}{\beta^2} \quad P_m^{*2} \tag{4}$$

Using the relationship for P_m^* given in Fig. 9 and using $W = \gamma W^*$, W and W* being the total energy in the laboratory system and center-of-mass system, respectively, Eq. (4) becomes

$$0 \gtreqless \frac{1}{\gamma^2-1}\left\{\left(\frac{W^2+\gamma^2(M^2-m^2)}{2\gamma W}\right)^2 - M^2\right\} - m^2. \tag{5}$$

Now, using $\beta = (P_i/W) = (P/W)$, $\gamma^2 = W^2/(W^2 - P^2)$, and after going through the algebra,

$$(W^2-P^2)^2 + (M^2-m^2)^2 - 4m^2W^2 - 2(M^2-m^2)(W^2-P^2) \lesseqgtr 0 \tag{6}$$

$$\begin{cases} <, \theta_m < 90^\circ \\ =, \theta_m = 90^\circ \\ >, \theta_m > 90^\circ. \end{cases}$$

Substituting into Eq. (6), $(W^2 - P^2) = 2Wm_o + m_i^2 - m_o^2$, $M^2 - m^2 = A$, and $m_i^2 - m_o^2 = C$,

$$4(m_o^2 - m^2)W^2 + 4m_o(C-A)W + (C-A)^2 \lessgtr 0, \quad (7)$$

or, multiplying by -1,

$$4(m^2 - m_o^2)W^2 - 4m_o(C-A)W - (C-A)^2 \equiv f(W,M,m,m_i) \gtrless 0$$

$$\begin{cases} >, \theta_m < 90^\circ \\ =, \theta_m = 90^\circ \\ <, \theta_m > 90^\circ. \end{cases} \quad (8)$$

For $M = m_i$ and $m = m_o$, i.e., $C = A$, $f(W....) = 0$, hence, no value of the energy for particle m_i will produce a laboratory angle of emission greater than 90° for a particle equal in mass to the mass of the target particle.

For other combinations of particle masses, things get more complex. Before proceeding with the analysis, an expression for the threshold energy in which particles of mass M and m can be produced will be derived. This energy is the energy in the center of mass system for which

$$W^* = M + m = W/\gamma$$

$$W^2 = \gamma^2(M + m)^2 = \frac{W^2}{W^2 - P^2}\ (M + m)^2$$

from which

$$W_{Th} = \frac{(M + m)^2 + m_o^2 - m_i^2}{2m_o} \quad . \tag{9}$$

Returning to the analysis for arbitrary masses, Eq. (8), by completing the square, becomes

$$f(W,M,m_1 m_i) = \left[W - \frac{m_o}{2(m^2-m_o^2)} (m_i^2 - m_o^2 + m^2 - M^2)\right]^2$$

$$- \frac{m^2}{4} \left(\frac{m_i^2 - m_o^2 + m^2 - M^2}{m^2 - m_o^2}\right)^2 \tag{10}$$

where $m \neq m_o$. Now, for application to the production of Λ^o-particles in π-meson-nucleon collisions, let $m_i = 0.140$ Bev, $m_o = 0.940$ Bev, and $m = 1.107$ Bev. As a function of W and M, Eq. (10) then becomes

$$f(W,M) = [W - 1.380\ (0.361 - M^2)]^2 - 2.635\ (0.361 - M^2)^2. \tag{11}$$

Eq. (11) represents a parabola which opens out in the direction of the positive f-axis. For M = 0, 0.361, and 1.00 Bev, Eq. (11) becomes

$$f(W,M = 0) = (W - 0.497)^2 - 0.343 \ , \tag{12}$$

$$f(W,\ M = 0.361) = W^2 \ , \tag{13}$$

and

$$f(W,\ M = 1.00) = (W + 0.881)^2 - 1.074 \ . \tag{14}$$

The corresponding values of the threshold energy are given by

$$W_{Th}\ (M = 0) = 1.11 \text{ Bev} \ , \tag{15}$$

$$W_{Th}\ (M = 0.361) = 2.00 \text{ Bev} \ , \tag{16}$$

and

$$W_{Th}\ (M = 1.00) = 2.88 \text{ Bev} \ , \tag{17}$$

respectively.

From Eqs. (12), (13), and (14) the maximum values of W for which $f(W) = 0$ are 1.052, zero, and 0.211 Bev. These values are less than the threshold energies given by Eqs. (15), (16), and (17), hence, it appears that $f(W,M) > 0$ for values of W above threshold. To test the function for large values of M, consider the values of W which make $f(W,M) = 0$ as determined from Eq. (11), or,

$$W(f = 0) = (1.380 \pm 1.62)\ (0.361 - M^2)\ .$$

As $M \to \infty$,

$$W(f = 0) \sim 0.2\ M^2\ . \qquad (18)$$

From Eq. (9), as $M \to \infty$,

$$W_{Th} \sim M^2/2m_o \sim 0.6\ M^2\ . \qquad (19)$$

Consequently, the threshold energy is always greater than the value of the energy, W, for which $f(W,M) = 0$. Hence, for a π-meson-nucleon collision, a Λ^o-particle produced in the interaction would not be seen moving backward in the laboratory system.

A similar analysis carried out for a nucleon-nucleon collision led to the same conclusion.

Therefore, the observation of Λ^o-particles moving backward in the laboratory system implies that the nucleus in which the particle was produced absorbed a large fraction of the momentum of the primary production particle.

IX. REFERENCES

1. L. Janossy, Cosmic Rays, 2nd Ed., Oxford At the Clavendon Press (1950).
2. E. J. Williams and G. E. Roberts, Nature, 145, 102 (1940).
3. A. Lovati, A. Mura, C. Succi, and G. Tagliaferri, Nuovo Cim., 12, No. 4, 526-38, (1954).
4. P. M. S. Blackett and G. P. S. Occhialini, Proc. Roy. Soc., A139, 699 (1933).
5. P. M. S. Blackett, Proc. Roy. Soc., A146, 281 (1934).
6. B. Rossi, Nature, 125, 636 (1930).
7. S. H. Neddermeyer and C. D. Anderson, Phys. Rev., 54, 88 (1938).
8. R. B. Leighton, C. D. Anderson, and A. J. Seriff, Phys. Rev., 75, 1432 (1949).
9. G. Salvini, Nuovo Cim., 8, 798-805 (1951).
10. H. S. Bridge, W. E. Hazen, B. Rossi, and R. W. Williams, Phys. Rev., 74, 1083 (1948).
11. M. J. Cohen, Rev. Sci. Instrum., 22, 966-77 (1951).
12. C. M. York, Jr., Phys. Rev., 96, 1635-37 (1954).
13. J. Keuffel and L. Mezzetti, Phys. Rev., 94, 794(A) (1954).
14. J. Linsley, Phys. Rev., 97, 1292 (1955).
15. R. B. Leighton, J. D. Sorrels, private communication.
16. C. G. Montgomery and D. D. Montgomery, Phys. Rev. 47, 429 (1935a); Phys. Rev., 48, 786 (1935b).

17. S. A. Korff, Phys. Rev., 56, 210 (1939).

18. K. H. Barker, et al., Phil. Mag., 44, 46-50 (1953).

19. A. L. Hodson, A. Loria and N. V. Ryder, Phil. Mag., 41, 826 (1950).

20. M. L. Merritt, Ph.D. Thesis, California Institute of Technology (1950).

21. R. C. Jopson, Ph.D. Thesis, California Institute of Technology (1950).

22. V. A. J. van Lint, Ph.D. Thesis, California Institute of Technology (1954).

23. G. H. Trilling, Ph.D. Thesis, California Institute of Technology (1955).

24. M. Schein and P. S. Gill, Rev. Modern Phys., 11, 267 (1939).

25. R. F. Christy and S. Kusaka, Phys. Rev., 59, 414 (1941).

26. B. Rossi, High-Energy Particles, Prentice Hall, New York (1952), pp. 16, 61.

27. B. Rossi, ibid., p. 259.

28. J. G. Wilson, ed., Progress in Cosmic Ray Physics, Interscience Publishers, Inc., New York (1952), pp. 403, 413.

29. B. Rossi, Chapter 5.

30. J. Blaton, Det. Kgl. Danske Videnskabernes Selskeb Matematisk--Fysiske Meddelelser, Bind XXIV, Nr. 20 (1950).

31. R. E. Lapp, Phys. Rev., 69, 321 (1946).

32. F. E. Driggers, Phys. Rev., 87, 1080 (1952).

33. W. Blocker, R. W. Kenney and W. K. H. Panofsky, Phys. Rev., 79, 419 (1950).

34. S. Belenky, J. Phys. U.S.S.R., 8, 305 (1944).